Acta Crystallographica Section F
Structural Biology and Crystallization Communications
ISSN 1744-3091

Structure of *Stenotrophomonas maltophilia* FeoA complexed with zinc: a unique prokaryotic SH3-domain protein that possibly acts as a bacterial ferrous iron-transport activating factor

Yi-Che Su,[a] Ko-Hsin Chin,[a,b] Hui-Chih Hung,[c] Gwan-Han Shen,[d] Andrew H.-J. Wang[e,f] and Shan-Ho Chou[a,b]*

[a]Institute of Biochemistry, National Chung-Hsing University, Taichung 40227, Taiwan, [b]National Chung Hsing University Biotechnology Center, National Chung-Hsing University, Taichung 40227, Taiwan, [c]Department of Life Sciences, National Chung-Hsing University, Taichung 40227, Taiwan, [d]Department of Internal Medicine, Taichung Veterans General Hospital, Taichung, Taiwan, [e]Core Facility for Protein Crystallography, Academia Sinica, Nankang, Taipei, Taiwan, and [f]Institute of Biological Chemistry, Academia Sinica, Nankang, Taipei, Taiwan

Correspondence e-mail: shchou@nchu.edu.tw

Received 11 March 2010
Accepted 15 April 2010

PDB Reference: FeoA, 3mhx.

Iron is vital to the majority of prokaryotes, with ferrous iron believed to be the preferred form for iron uptake owing to its much better solubility. The major route for bacterial ferrous iron uptake is found to be *via* an Feo (**fe**rrous ir**o**n-transport) system comprising the three proteins FeoA, FeoB and FeoC. Although the structure and function of FeoB have received much attention recently, the roles played by FeoA and FeoC have been little investigated to date. Here, the tertiary structure of FeoA from *Stenotrophomonas maltophilia* (*Sm*), a vital opportunistic pathogen in immunodepressed hosts, is reported. The crystal structure of *Sm*FeoA has been determined to a resolution of 1.7 Å using an Se single-wavelength anomalous dispersion (Se-SAD) approach. Although *Sm*FeoA bears low sequence identity to eukaryotic proteins, its structure is found to adopt a eukaryotic SH3-domain-like fold. It also bears weak similarity to the C-terminal SH3 domain of bacterial DtxR (diphtheria toxin regulator), with some unique characteristics. Intriguingly, *Sm*FeoA is found to adopt a unique dimer cross-linked by two zinc ions and six anions (chloride ions). Since FeoB has been found to contain a G-protein-like domain with low GTPase activity, FeoA may interact with FeoB through the SH3–G-protein domain interaction to act as a ferrous iron-transport activating factor.

1. Introduction

Iron is vital to the majority of prokaryotes, which have therefore developed a variety of iron-transport pathways to compete with their hosts for iron supplies (Andrews *et al.*, 2003). The most common pathways employed by bacteria appear to be those transporting ferric complexes, such as ferric siderophores, ferric transferrin, ferric citrate *etc.* (Andrews *et al.*, 2003). However, ferrous iron is now believed to be the preferred form for iron uptake owing to its much better solubility (0.1 *M* for Fe^{2+} *versus* 10^{-18} *M* for Fe^{3+} at pH 7) and the major route for its uptake has now been found to take place *via* an Feo (**ferro**us iron-transport) system that differs considerably from ferric iron-transport systems (Kammler *et al.*, 1993; Velayudhan *et al.*, 2000; Cartron *et al.*, 2006). The Feo system is known to comprise three genes, which are likely to form an *feo*ABC operon (Hantke, 2003). FeoA is a small protein of approximately 75 residues with unknown function, while FeoB is a large protein of 773 residues that contains an integral membrane domain that is likely to act as a ferrous permease (Velayudhan *et al.*, 2000; Marlovits *et al.*, 2002; Hantke, 2003; Koster *et al.*, 2009) and a GDP-dissociation inhibitor (GDI) domain for stabilizing GDP binding (Eng *et al.*, 2008; Hattori *et al.*, 2009) and FeoC is another small protein that contains an Fe–S cluster that possibly serves as a transcriptional regulator for the *feo*ABC operon. In the NCBI database, most *feo*A-like genes are adjacent to *feo*B genes, indicating that their functions are strictly associated (Cartron *et al.*, 2006).

Stenotrophomonas maltophilia (*Sm*) has emerged as an important opportunistic pathogen in immunodepressed hosts (Safdar & Rolston, 2007; Looney *et al.*, 2009). It has recently been described as a 'superbug' because it is resistant to almost all antibiotics. This phenomenon has caused tremendous concern and extreme difficulty in treating its infections (Johnson & Duckworth, 2008). Although there has been some progress in this respect (for example, its genome sequence has recently been completed and revealed numerous drug-

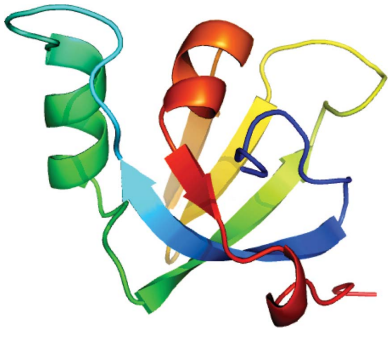

Table 1
Statistics of data-collection and structure refinement for SeMet *Sm*FeoA.

Values in parentheses are for the outermost shell.

Beamline	NSRRC BL13B1
Data collection	
Wavelength (Å)	0.97962
Space group	$P2_12_12_1$
Unit-cell parameters (Å, °)	a = 46.015, b = 54.031, c = 61.035, $\alpha = \beta = \gamma = 90$
Resolution range (Å)	30–1.7 (1.76–1.7)
Total observations	159867
Unique observations	17106 (1499)
Redundancy	9.3 (9.2)
Completeness (%)	98.8 (90.0)
R_{merge} (%)	7 (38)
$I/\sigma(I)$	23.4 (5.9)
R_{free} test-set size (%)	5
Refinement statistics	
R (%)	19
R_{free} (%)	22
Model content	
Protein residues	160
Water molecules	156
Chloride ions	6
Zinc ions	2
R.m.s deviations from ideal geometry	
Bond lengths (Å)	0.0045
Bond angles (°)	1.257
Solvent content (%)	53

resistance determinants; Crossman *et al.*, 2008), structural studies of proteins encoded by this bacterium are still scarce. Here, we report the tertiary structure of *Sm*0974 determined to a resolution of 1.7 Å using X-ray crystallography. Although no clear sequence identity to eukaryotic SH3-domain proteins can be found, the final structure of *Sm*0974 was found to adopt an SH3-domain-like fold similar to that adopted by eukaryotic proteins (Mayer, 2001). Since the eukaryotic SH3 domain is well known for its capability to mediate protein–protein interactions (Mayer, 2001), this has led to the suggestion that FeoA may interact with FeoB to regulate FeoB-dependent ferrous iron-uptake activity (Cartron *et al.*, 2006). Interference with the FeoA–FeoB interaction may constitute a novel approach for treating *S. maltophilia* infection, owing to the importance of ferrous iron as an essential element in bacteria.

2. Materials and methods

2.1. Cloning, expression and purification of *Sm*FeoA

The *Sm*FeoA gene was PCR-amplified directly from the human pathogen *S. maltophilia* using the forward primer 5′-TACTTCCA-ATCCAATGCTATGACGCTGTCCGAACTG-3′ and the reverse primer 5′-TTATCCACTTCCAATGTCATGCGCGTCGTTCCTG-3′ to form a fragment of the required length. The PCR fragment was confirmed to have the correct size by DNA sequencing. A ligation-independent cloning (LIC) approach using the pMCSG7 expression vector (Aslanidis & de Jong, 1990; Stols *et al.*, 2001) was used to obtain the desired constructs. The final construct coded for an N-terminal His_6 tag, a 17-amino-acid linker and the *Sm*FeoA target under the control of the T7 promoter. Overexpression of the His_6-tagged target protein was induced by the addition of 0.5 m*M* IPTG at 293 K for 20 h in *Escherichia coli* BL21 host strain. The cells were harvested, resuspended in lysis buffer (80 m*M* Tris–HCl pH 8.0, 250 m*M* NaCl) and lysed using a microfluidizer (Microfluidics). Most of the target protein was found to be present in the soluble fraction after centrifugation. The target protein was purified by immobilized metal-affinity chromatography (IMAC) on a nickel column (Sigma) and was eluted with a gradient of 50–300 m*M* imidazole in lysis buffer. The fractions containing *Sm*FeoA were monitored by SDS–PAGE, recombined and dialyzed repeatedly against lysis buffer. After concentration, the His_6 tag and linker were cleaved from *Sm*FeoA using tobacco etch virus (TEV) protease at 277 K for 16 h and removed by IMAC. For crystallization, *Sm*FeoA protein was further purified by FPLC (ÄKTA, Pharmacia Inc.) on a Superdex 200 column equilibrated with lysis buffer. The final fresh target protein exhibited a purity of greater than 99% and contained only an extra tripeptide (SNA) at the N-terminal end. SeMet-labelled *Sm*FeoA was prepared in a similar way and was produced using *E. coli* strain BL21 (DE3) as the host in the absence of methionine but with ample amounts of SeMet (100 mg l^{-1}). The medium consisted of 1 g NH_4Cl, 3 g KH_2PO_4 and 6 g Na_2HPO_4 supplemented with 20%(*w*/*v*) glucose, 0.3%(*w*/*v*) $MgSO_4$ and 10 mg $FeSO_4$ in 1 l double-distilled water. Induction was conducted at 293 K for 24 h by the addition of 0.5 m*M* IPTG. Purification of the SeMet-labelled *Sm*FeoA protein was performed using the protocols established for the native protein.

2.2. Crystallization of *Sm*FeoA

For crystallization, native protein was concentrated to 8 mg ml^{-1} in 80 m*M* Tris–HCl, 250 m*M* NaCl using an Amicon Ultra-10 (Millipore). Screening for crystallization conditions was performed using sitting-drop vapour diffusion in 96-well plates (Hampton Research) at 277 K by mixing 0.5 µl protein solution with 0.5 µl reagent solution. Initial screens including the Hampton Clear Strategy Screen 1, Structure Screens 1 and 2, a systematic PEG–pH screen and the PEG/Ion Screen were performed using a Gilson C240 crystallization workstation. Needle-like crystals appeared in one week from reservoir solution comprising 20%(*w*/*v*) PEG 3000, 0.2 *M* zinc acetate, 0.1 *M* imidazole pH 8.0; the crystals were about 0.02 × 0.01 × 0.01 mm in size. Crystals suitable for diffraction experiments were grown by mixing 1.5 µl protein solution with 1.5 µl reagent solution at 298 K and reached dimensions of 0.2 × 0.02 × 0.02 mm after one week. SeMet-labelled *Sm*FeoA was crystallized in 25%(*v*/*v*) PEG 550 MME, 0.1 *M* MES, 0.01 *M* zinc sulfate pH 6.5; the crystal size was 0.2 × 0.03 × 0.03 mm.

2.3. Data collection

Crystals were flash-cooled at 100 K in a stream of cold nitrogen. X-ray diffraction data were collected on the National Synchrotron Radiation Research Center (NSRRC) beamline 13B1, Taiwan. A selenomethionine single-wavelength SAD data set to 1.7 Å resolution was obtained. The data were indexed and integrated using the *HKL*-2000 processing software (Otwinowski & Minor, 1997), giving a data set that was approximately 98.8% complete with an overall R_{merge} of 7% on intensities. Refinement of Se-atom positions, phase calculation and density modification were performed using *SOLVE*/*RESOLVE* (Terwilliger & Berendzen, 1999). The model was manually adjusted using the *XtalView*/*Xfit* package (McRee, 1999). *CNS* (Brünger *et al.*, 1998) was then used for refinement to a final R_{cryst} of 19% and an R_{free} of 22%.

3. Results and discussion

3.1. The tertiary structure of *Sm*0974

A bioinformatics study indicated that *Sm*0974 belonged to the bacterial FeoA protein family (http://sm.life.nthu.edu.tw/); it contained 84 amino-acid residues with an alkaline pI of 9.43. Its crystal structure was determined to a resolution of 1.7 Å using an Se-SAD approach. The crystals belonged to space group $P2_12_12_1$ and

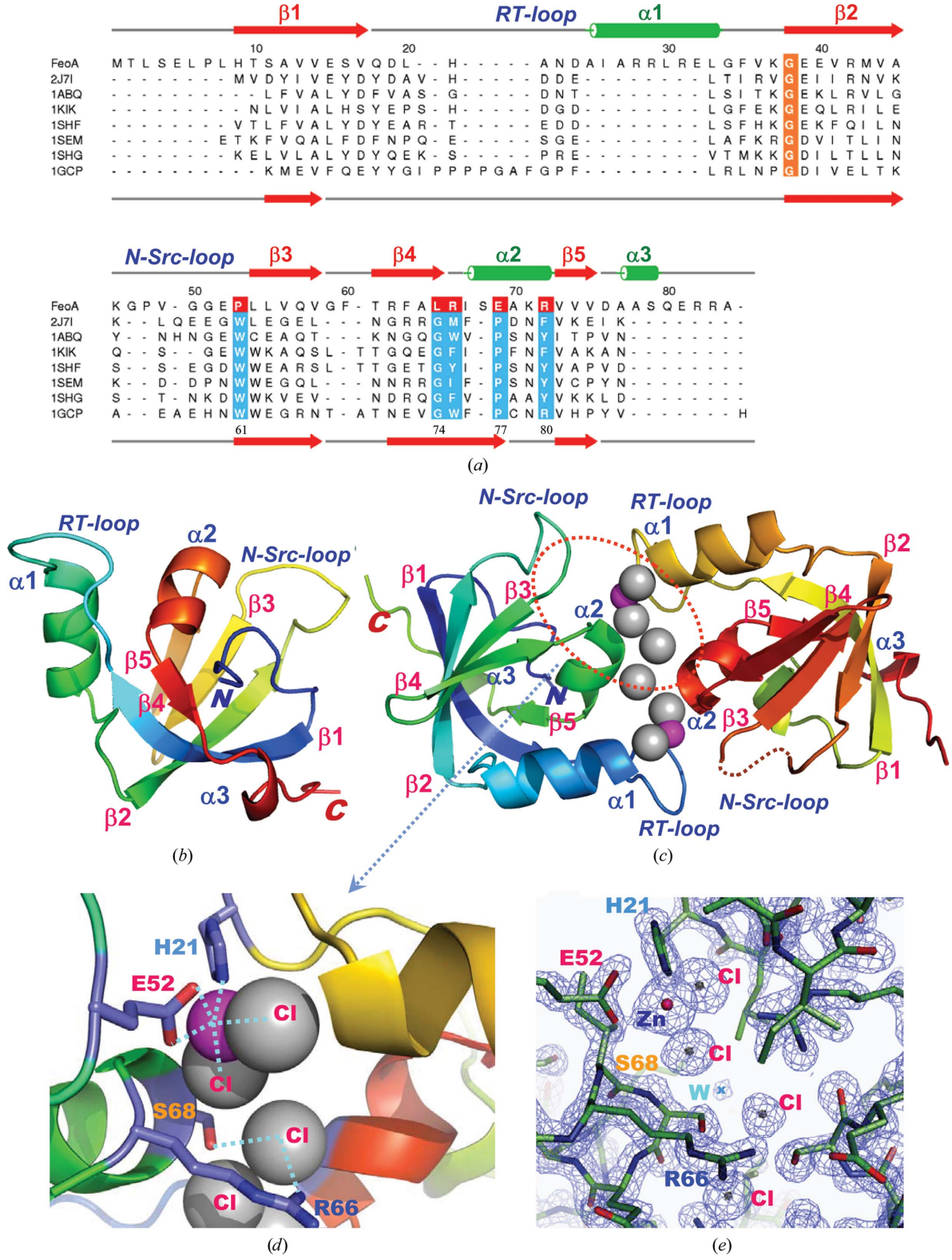

Figure 1
Sequence and tertiary structure of *Sm*FeoA. (*a*) Sequence and structural alignment of *Sm*FeoA with eukaryotic SH3 domains. A glycine residue at the start of strand *β*2 is conserved in all SH3 domains and is highlighted in orange, while amino-acid residues that are well conserved in eukaryotic SH3 domains but are altered in *Sm*FeoA are highlighted in blue and red, respectively. The secondary-structural elements are annotated accordingly for *Sm*FeoA (above) and 1gcp (below), respectively. (*b*) The tertiary structure drawn in cartoon representation and coloured in a rainbow from blue (N-terminus) to red (C-terminus). (*c*) The dimeric *Sm*FeoA structure as observed in the crystal. The two monomers are symmetrically related by a *C*2 axis perpendicular to the plane and are cross-linked by two zinc ions (shown as magenta spheres) and six chloride ions (shown as grey spheres). (*d*) An enlargement of the circled region in (*c*). The residues participating in coordination with the zinc ion are drawn in stick representation and annotated by residue number. The zinc ion is coordinated by the side-chain atoms of His12 and Glu52 and two chloride ions to form a tetrahedral geometry. (*e*) The corresponding $2F_o - F_c$ electron-density map of Fig. 1(*d*) drawn at a 1σ contour level. The map regions of interest are annotated. The electron density of a water molecule, which is much smaller than those of chloride ions, is annotated by a letter 'W'.

contained two *Sm*0974 molecules per asymmetric unit. The Matthews coefficient and solvent content (Otwinowski & Minor, 1997) of the crystals were 2.1 Å^3 Da^{-1} and 53%, respectively. The data and final refinement statistics are summarized in Table 1. The final *Sm*FeoA structure adopts a eukaryotic SH3 fold that is rarely observed in the bacterial kingdom (Whisstock & Lesk, 1999). It starts with an N-terminal coil (1–8), which is followed by β-strand β1 (9–17), α-helix α1 (25–33), β-strand β2 (38–45), β-strand β3 (54–58), β-strand β4 (61–65), α-helix α2 (67–72) and β-strand β5 (73–75) and finally by a 3_{10}-helix (77–79) and a C-terminal coil (80–84), as shown in Figs. 1(*a*) and 1(*b*). Interestingly, *Sm*FeoA is found to adopt a dimer that is cross-linked by two zinc ions and six chloride ions. Initially, numerous unexpected electron-density-rich regions were observed in the map (Fig. 1*e*). From the spherical shapes in the map, we suspected that these were likely to arise from the contribution of ions. Since the crystals of *Sm*FeoA were obtained using zinc sulfate and sodium chloride as additives during screening and because one glutamate residue and one histidine residue were found to be situated near to the unknown electron density, we suspected that these regions originated from zinc ions. This notion was found to be correct after iterative structural refinement and was finally confirmed in the $F_o - F_c$ map, in which the intensity proposed to arise from zinc ions was no longer present (data not shown). The identity of the zinc ion was also validated by atomic absorption spectrophotometry data (not shown). In addition to zinc ions, six regions of spherical electron density close to the two zinc ions were also found in the map (Figs. 1*c* and 1*e*). At first, water molecules were fitted into the unknown density map. However, some residual electron density remained in the final $F_o - F_c$ map and could not be cancelled out even after repeated calculations. Finally, when chloride ions were employed a perfect fit was achieved and residual electron density was no longer observed in the final map. Therefore, these six unknown electron-density-rich regions are believed to arise from chloride ions. In fact, the electron densities of waters were found to be much smaller than those of chloride ions in the final map (one example is marked by an 'x' in Fig. 1*e*). The *Sm*FeoA monomers are thus cross-linked *via* the zinc and chloride ions to form a dimer in the crystal. Extensive interactions are present in the interface between the ions and the amino acids in the three loops and are shown in Figs. 1(*b*) and 1(*c*). The zinc ions are found to adopt a tetrahedral coordination *via* the bifurcate carboxylate O atoms of Glu52 in the N-Src loop, the imidazole N atom of His21 in the RT loop and two chloride ions (Fig. 1*d*). Furthermore, two extra chloride ions are found to separate the two zinc tetrahedral coordination environments, with each chloride ion forming a hydrogen bond to the side-chain O atom of Ser68 and a salt bridge with the guanido N atom of Arg66 in the β4–α2 loop region (Fig. 1*d*). It is intriguing to note that the coordination of metal ion by anions is rather rare but is not without precedents. For example, a metal-mediated dimerization was also observed in the RNA-editing enzyme adenosine deaminase, with a chloride ion found to participate in forming an octahedron (Athanasiadis *et al.*, 2005). Similarly, a sulfate or phosphate ion was also found to be involved in coordinating the metal ion in diphtheria toxin repressor (Pohl *et al.*, 2001).

3.2. Structural comparisons of *Sm*FeoA with other eukaryotic SH3 domains

Sequence and structural alignment of prokaryotic *Sm*FeoA with eukaryotic SH3 domains such as PDB entries 2j7i (cyan; Moncalian *et al.*, 2006), 1abq (pink; Musacchio *et al.*, 1994), 1gcp (green; Nishida *et al.*, 2001), 1kik (yellow; Briese & Willbold, 2003), 1sem (blue; Lim *et al.*, 1994), 1shf (magenta; Noble *et al.*, 1993) and 1shg (orange; Musacchio *et al.*, 1992) are shown in Figs. 1(*a*) and 2, respectively. It is clear from the structural alignment that while *Sm*FeoA exhibits a similar fold to those of the eukaryotic proteins, considerable differences also exist between the two. The most prominent differences are located in three regions, namely the RT loop, the N-Src loop and the β4–α2 linker. In the RT-loop region, while the eukaryotic SH3 domains feature a shorter loop turning away from the viewer, that of *Sm*FeoA features a longer loop pointing towards the viewer (the left side in Fig. 2). Also, unlike other eukaryotic SH3 domains, the C-terminal end of the RT loop in *Sm*FeoA is found to adopt a helix of $2\frac{1}{2}$ turns (the *Sm*FeoA structure is shown in cartoon representation in red in Fig. 2, while all others are shown as line representations in various colours). In the N-Src-loop region, in contrast, that of the *Sm*FeoA is found to turn away from the viewer, while those of eukaryotic SH3 domains point towards the viewer (right side of Fig. 2). Also, in the β4–α2 linker region the top part of the linker in *Sm*FeoA is found to adopt a helix, while those of other eukaryotic SH3 domains adopt a coil. Since it is generally believed that these

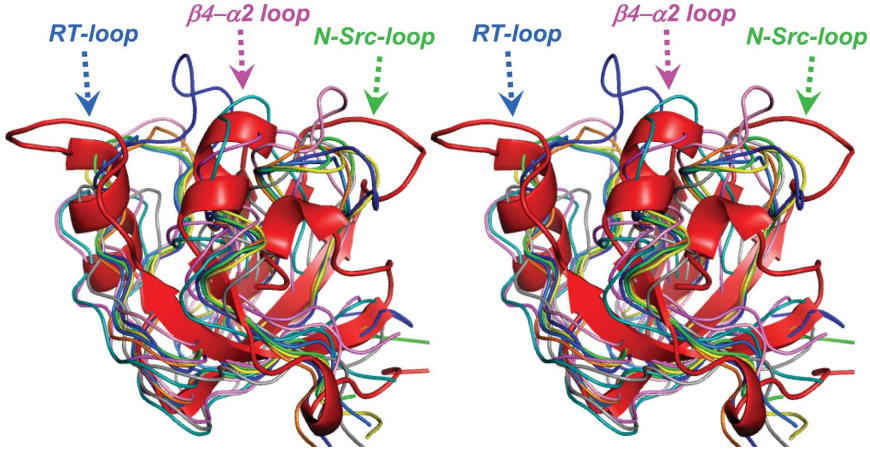

Figure 2
Superimposition in stereo of the *Sm*FeoA structure (coloured red) with other published eukaryotic SH3-domain structures (1abq, pink, r.m.s.d. 1.43 Å for 27 C$^\alpha$ atoms; 1gcp, blue, r.m.s.d. 1.35 Å for 27 C$^\alpha$ atoms; 1kik, orange, r.m.s.d. 1.46 Å for 26 C$^\alpha$ atoms; 1sem, green, r.m.s.d. 1.35 Å for 28 C$^\alpha$ atoms; 1shf, grey, r.m.s.d. 2.16 Å for 21 C$^\alpha$ atoms; 1shg, light purple, r.m.s.d. 1.96 Å for 14 C$^\alpha$ atoms; 2j7i, teal, r.m.s.d. 1.46 Å for 24 C$^\alpha$ atoms). Only the *Sm*FeoA structure is shown in cartoon representation, while all other eukaryotic SH3 domains are shown as lines. It is clear from the comparison that although the *Sm*FeoA structure is globally similar to other eukaryotic SH3 domains, significant differences are observed in three regions, the RT loop, the β4–α2 linker and the N-Src loop, which are marked by blue, red and green dotted arrows in the figure, respectively.

loops may play important roles in conferring the SH3 domain with the ability to act as a special interaction platform for proline-rich peptides, the dramatically different loop conformations observed in the prokaryotic *Sm*FeoA SH3 domain indicate that it may interact with proteins of a different nature. In fact, the sequence similarity shared by the eukaryotic SH3 domains at several highly conserved positions such as Trp61, Gly74, Trp75 and Pro77 (named according to the 1gcp sequence) is altered to residues of rather different nature (Pro53, Leu65, Arg66 and Glu69) in *Sm*FeoA (highlighted in blue and red, respectively, in Fig. 1*a*). Taken together, these different sequence and structure characteristics between the prokaryotic and eukaryotic SH3 domains indicate that they may assume distinct functions. Further studies of the interaction partners of prokaryotic SH3 domains are necessary in order to clarify this issue.

3.3. Structural comparison of *Sm*FeoA with the C-terminal domains of DtxR repressors

Although it is uncommon to find SH3 domains in the bacterial kingdom (Whisstock & Lesk, 1999), the C-terminal domain of the diphtheria toxin repressor (DtxR) from *Corynebacterium diphtheriae* has nevertheless been found to adopt an SH3 domain in the presence of cobalt or manganese ions (Qiu *et al.*, 1996). The structure of an intramolecular complex (PrSH3) formed between the N-terminal proline-rich segment and the SH3 domain of DtxR has also been solved by NMR spectroscopy (Wylie *et al.*, 2005). Some interesting structural features of the free SH3 and PrSH3 domains have been noted from these studies. For example, the proline-rich segment was found not to adopt a PPII (pseudosymmetrical polyproline class II) helix conformation (Kang *et al.*, 2000), but an extended coil that was still able to bind to the DtxR SH3 domain using the similar PPII recognition cavity. Additionally, the conserved aromatic amino-acid residues (Trp61 and Trp75 in Fig. 1*a*) present in the eukaryotic SH3 domain that are crucial for protein interaction were not detected as being conserved in the hydrophobic core of the prokaryotic SH3 β-barrel domain (Wylie *et al.*, 2005). These results indicate that prokaryotic SH3 domains may exhibit structural and functional characteristics that are unique to the bacterial kingdom. Comparison of the *Sm*FeoA structure with those reported for the DtxR SH3-domain and DtxR PrSH3 structures revealed further structural variations in the prokaryotic SH3 domain, as shown in Figs. 3(*a*) and 3(*b*). From the comparison, it is clear that they do adopt a common prokaryotic SH3 fold, with a number of conserved residues in the hydrophobic core, such as Leu3, Leu6, Ala12, Val14, Val17, Val41,

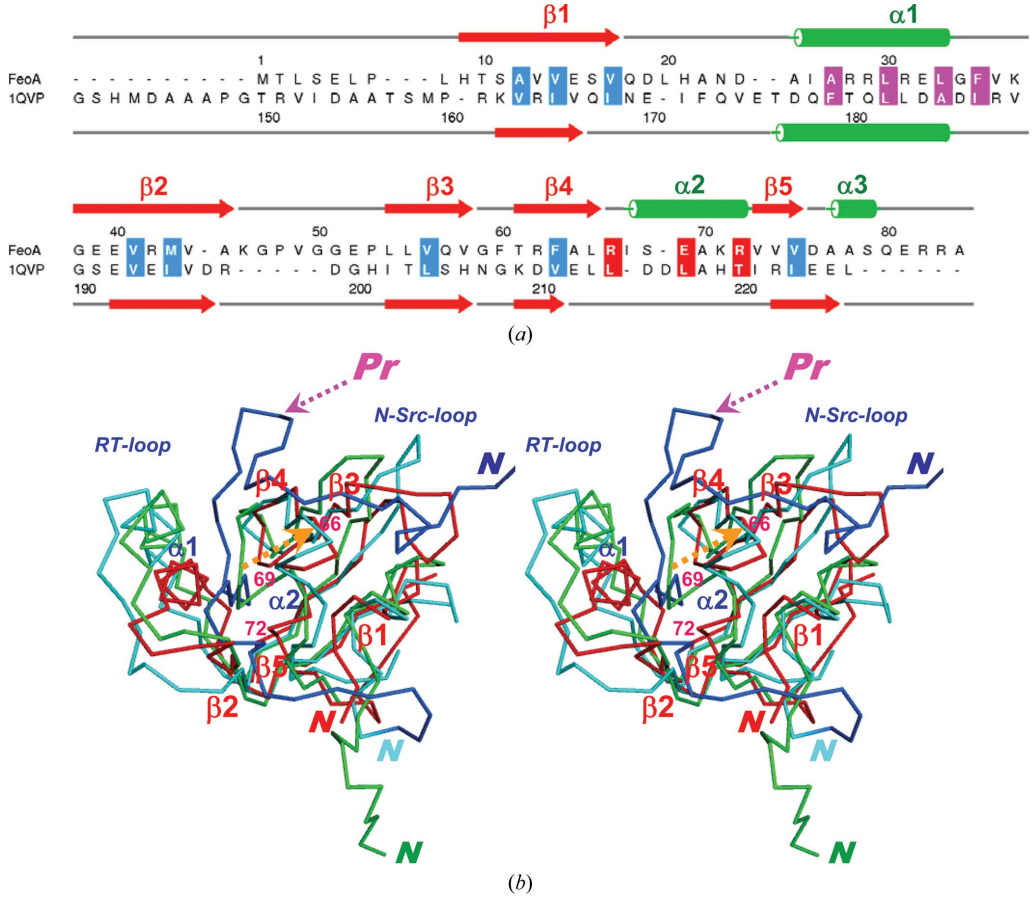

Figure 3
Comparison of the *Sm*FeoA structure with prokaryotic DxtR SH3 or DxtR PrSH3 domains. (*a*) Sequence and structural alignment between the *Sm*FeoA structure and the DxtR SH3 domain. The secondary-structural elements are annotated for *Sm*FeoA (above) and 1qw1 (Wylie *et al.*, 2005; below). Similar hydrophobic residues between the β-barrels of the two SH3 domains are highlighted in blue and those in helix α1 are highlighted in purple, while the three residues in and near helix α2 are changed from Leu213, Leu217 and Thr220 in the DxtR SH3 domain to Arg66, Glu69 and Arg72 in *Sm*FeoA, respectively, and are highlighted in red. (*b*) Superimposition of the *Sm*FeoA, DxtR SH3 (1qvp; Wylie *et al.*, 2005) and DxtR PrSH3 (1qw1) structures drawn in C^{α} representation and shown in stereo. *Sm*FeoA is coloured red and DxtR SH3 green, while the C-terminal SH3 domain of DxtR PrSH3 is shown in cyan and the N-terminal Pr domain in blue (also marked by a red dotted arrow). Intriguingly, the β4 strand in the apo DxtR SH3 domain is close to the α1 helix. However, in the intramolecular PrSH3 complex the β4 strand is found to shift considerably towards the β3 strand (indicated by an orange dotted arrow) to leave room for insertion of the Pr peptide into the cavity between the α1 helix and the β4 strand. The β4 strand in PrSH3 can now superimpose well with that of *Sm*FeoA.

Met43, Val56, Phe63 and Val75 (numbered according to the *Sm*FeoA sequence and highlighted in blue in Fig. 3*a*) and with well superimposed $\beta1$–$\beta2$–$\beta3$–$\beta5$ strands (Fig. 3*b*, labelled in red). However, notable differences also exist between the *Sm*FeoA structure and that of the DxtR SH3 domain. Firstly, the apo form of *Sm*FeoA adopts a conformation that is more akin to that of the intramolecular DxtR PrSH3 complex form, with well superimposed $\beta4$ strands (coloured red and cyan, respectively, in Fig. 3*b*). In the DxtR SH3 domain, its $\beta4$ strand (coloured green in Fig. 3*b*) shifts approximately 5 Å towards the $\alpha1$ helix, shortening the width of the cavity and potentially blocking the insertion of the Pr linker into the recognition cavity. A structural reorganization is thus necessary to open up the cavity to accommodate the Pr peptide (coloured blue and annotated by a pink dotted arrow in Fig. 3*b*). *Sm*FeoA thus seems to adopt a conformation that is better adapted to interacting with its binding partner. However, detailed structural analyses indicated that a different type of structural reorganization may still be necessary for *Sm*FeoA to interact with its partner, owing to two characteristic features of *Sm*FeoA. The first is that three long-chain charged amino acids, namely Arg66, Glu69 and Arg72 (highlighted in red in Fig. 3*a* and numbered at the C^{α} positions in Fig. 3*b*), were found to replace the original hydrophobic amino acids situated in the helical $\alpha2$ region. The Arg66 and Arg72 amino acids were found to exhibit severe steric hindrance towards the Pr peptide when the DxtR PrSH3 domain was superimposed on *Sm*FeoA. Similarly, the $\alpha1$ helix of *Sm*FeoA was also found to be located nearer to the $\beta2$ strand, causing further potential steric hindrance with the Pr peptide (on the left side of Fig. 3*b*), although it contains similar hydrophobic residues that can interact with the Pr peptide as in DxtR SH3 (residues highlighted in pink in Fig. 3*a*). These two characteristic structural features of *Sm*FeoA will restrict the potential peptide binding in the cavity region of *Sm*FeoA unless another alternative binding mode is employed. The *Sm*FeoA structure thus represents a novel variant of the prokaryotic SH3 domain.

To date, no tertiary structure of FeoA has been published, although the FeoA coordinates from several bacterial species have been deposited in the PDB, including those from *Thermococcus thioreducens* (PDB code 3e19; 31% sequence identity; R. C. Hughes, Y. Li, B.-C. Wang, Z.-J. Liu & J. D. Ng, unpublished work) determined by X-ray crystallography and those from *Clostridium acetobutylicum* (PDB code 2k4y; 31% sequence identity; K. Singarapu, Y. Wu, J. Hua, D. Sukumaran, L. Zhao, M. Jiang, E. L. Foote, R. Xiao, R. Nair, M. C. Baran, G. V. T. Swapna, T. Acton, B. Rost, G. T. Montelione & T. Szyperski, unpublished work), *C. thermocellum* (2k5l and 2k5i; 29% sequence identity; A. Zeri, K. K. Singarapu, J. L. Mills, Y. Wu, E. Garcia, H. Wang, M. Jiang, E. L. Foote, R. Xiao, R. Nair, J. K. Everett, G. V. T. Swapna, T. B. Acton, B. Rost, G. T. Montelione & T. Szyperski, unpublished work; G. Liu, R. Xiao & G. T. Montelione, unpublished work), *Chlorobium tepidum* (2k5f; 34% sequence identity; A. Eletsky, B. Sathyamoorthy, J. L. Mills, A. Zeri, L. Zhao, K. Hamilton, E. L. Foote, R. Xiao, R. Nair, M. C. Baran, G. V. T. Swapna, T. B. Acton, B. L. Rost, G. T. Montelione & T. Szyperski, unpublished work) and *Klebsiella pneumoniae* (2gcx; no significant identity; K.-W. Hung, C.-C. Cheng, T.-H. Yu, S.-H. Wang, C.-F. Chang, S.-F. Tsai & T.-H. Huang, unpublished work) determined using NMR. A superimposition of these FeoA structures is shown in Fig. 4. The 3e19 crystal structure was determined to a good resolution (2.0 Å) and superimposes well with that of *Sm*FeoA (r.m.s.d. of 1.16 Å between 61 of 84 C^{α} atoms), yet they exhibit two major structural differences: the RT loop of 3e19 moves backwards (looking from the loop

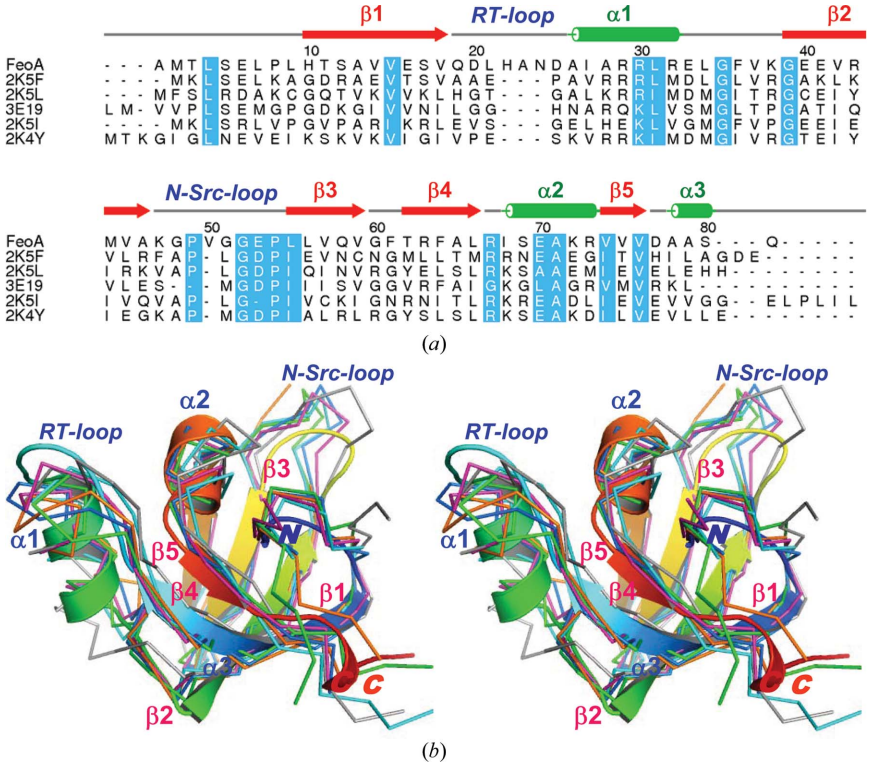

Figure 4
Sequence alignments and structural overlap of the *Sm*FeoA structure (rainbow) with other deposited FeoA structures from *Thermococcus thioreducens* (PDB code 3e19, orange), *Clostridium acetobutylicum* (2k4y, green), *C. thermocellum* (2k5i, blue; 2k5l, magneta), *Chlorobium tepidum* (2k5f, cyan) and *Klebsiella pneumoniae* (2gcx, grey) shown in stereo. The FeoA sequence from *K. pneumoniae* was not included in the sequence comparison owing to its greater variation. The secondary-structural elements are annotated as in Fig. 1.

interface shown in Figs. 1*b* and 1*c*) by approximately 5 Å and residues 48 and 49 in the N-Src loop of 3e19 are not visible. This situation differs from that in *Sm*FeoA, in which the entire loop containing residues Gly47-Pro48-Val49-Gly50-Gly51-Glu52 is well observed. These differences possibly arise from the fact that no metal ions are observed in the 3e19 structure, which may result in more flexible RT and N-Src loops. Since the loops of SH3 domains are presumably responsible for interacting with other proteins, the clear observation of loop structure in FeoA may be important in detecting conformational changes associated with FeoB binding. The crystal structure of *Sm*FeoA exhibits larger r.m.s.d. values from the FeoA structures determined by NMR, which range from 1.32 Å for 43 C^{α} atoms (2k5i) to 1.76 Å for 66 C^{α} atoms (2gcx). The RT loop and N-Src loop of those structures determined by NMR also experience different degrees of shift to those in *Sm*FeoA. It is unclear at present whether these structural differences in the loops play any biological role.

FeoA protein bears no clear sequence similarity to the prokaryotic DtxR (8.2% identity) and eukaryotic SH3 domains (9.0% identity), but their common fold does suggest a possible similar role in mediating protein–protein interactions. Since the activities of GTPases (molecular switches) have generally been found to be enhanced by GTPase-activating proteins (GAPs) that possess SH3 domains (Siderovski & Willard, 2005; Cartron *et al.*, 2006) and the FeoB protein was found to possess G-protein domains with low GTPase activity (Marlovits *et al.*, 2002; Hantke, 2003; Eng *et al.*, 2008; Koster *et al.*, 2009), it has been suggested that FeoA may act as a GAP to stimulate the GTPase activity and Fe^{2+} uptake of FeoB in an SH3-dependent manner (Cartron *et al.*, 2006). Owing to the important roles played by ferrous ion, interference with the *Sm*FeoA–*Sm*FeoB interaction may constitute a novel approach for treating *S. maltophilia* infection without the danger of eliciting drug resistance (Hughes, 2003). A cocrystal study of the *Sm*FeoA–*Sm*FeoB complex is necessary to elucidate this notion.

To date, no FeoA homodimer has been reported. However, a human Lck-SH3 domain was found to form a homodimer induced by zinc ions (Romir *et al.*, 2007). Interestingly, such dimerization was also found to compete with the binding of proline-rich motifs. The dimerization process was therefore proposed to be a possible mechanism by which Lck activity was modulated. However, we found that *Sm*FeoA existed mainly as a monomer even at high zinc-ion concentrations when running gel-filtration column chromatography and analytical ultracentrifugation (data not shown). The importance of the *Sm*FeoA dimer in the crystal thus remains to be elucidated.

This work was supported by an Academic Excellence Pursuit grant from the Ministry of Education and by the National Science Council, Taiwan, Republic of China (grant 97-2113-M005-005-MY3) to S-HC. We appreciate the service of the Structural Genomics Databases provided by the GMBD Bioinformatics Core (http//www.tbi.org.tw), NRPGM, Taiwan. We would also like to thank the Core Facilities for Protein X-ray Crystallography in the Academia Sinica, Taiwan for help in crystal screening and the National Synchrotron Radiation Research Center (NSRRC) in Taiwan and the SPring-8 Synchrotron facility in Japan for assistance during X-ray data collection. The National Synchrotron Radiation Research Center is a user facility supported by the National Science Council, Taiwan, Republic of China and the Protein Crystallography Facility is supported by the National Research Program for Genomic Medicine, Taiwan, Republic of China.

References

Andrews, S. C., Robinson, A. K. & Rodriguez-Quinones, F. (2003). *FEMS Microbiol. Rev.* **27**, 215–237.
Aslanidis, C. & de Jong, P. J. (1990). *Nucleic Acids Res.* **18**, 6069–6074.
Athanasiadis, A., Placido, D., Maas, S., Brown, B. A. II, Lowenhaupt, K. & Rich, A. (2005). *J. Mol. Biol.* **351**, 496–507.
Briese, L. & Willbold, D. (2003). *BMC Struct. Biol.* **3**, 3.
Brünger, A. T., Adams, P. D., Clore, G. M., DeLano, W. L., Gros, P., Grosse-Kunstleve, R. W., Jiang, J.-S., Kuszewski, J., Nilges, M., Pannu, N. S., Read, R. J., Rice, L. M., Simonson, T. & Warren, G. L. (1998). *Acta Cryst.* D**54**, 905–921.
Cartron, M. L., Maddocks, S., Gillingham, P., Craven, C. J. & Andrews, S. C. (2006). *Biometals*, **19**, 143–157.
Crossman, L. C. *et al.* (2008). *Genome Biol.* **9**, R74.
Eng, E. T., Jalilian, A. R., Spasov, K. A. & Unger, V. M. (2008). *J. Mol. Biol.* **375**, 1086–1097.
Hantke, K. (2003). *Trends Microbiol.* **11**, 192–195.
Hattori, M., Jin, Y., Nishimasu, H., Tanaka, Y., Mochizuki, M., Uchiumi, T., Ishitani, R., Ito, K. & Nureki, O. (2009). *Structure*, **17**, 1345–1355.
Hughes, D. (2003). *Nature Rev. Genet.* **4**, 432–441.
Johnson, A. P. & Duckworth, G. J. (2008). *Br. Med. J.* **336**, 1322.
Kammler, M., Schon, C. & Hantke, K. (1993). *J. Bacteriol.* **175**, 6212–6219.
Kang, H. O., Freund, C., Duek-Cohan, J. S., Musacchio, A., Wagner, G. & Rudd, C. E. (2000). *EMBO J.* **19**, 2889–2899.
Koster, S., Wehner, M., Herrmann, C., Kuhlbrandt, W. & Yildiz, O. (2009). *J. Mol. Biol.* **392**, 405–419.
Lim, W. A., Richards, F. M. & Fox, R. O. (1994). *Nature (London)*, **372**, 375–379.
Looney, W. J., Narita, M. & Muhlemann, K. (2009). *Lancet Infect. Dis.* **9**, 312–323.
Marlovits, T. C., Haase, W., Herrmann, C., Alter, S. G. & Unger, V. M. (2002). *Proc. Natl Acad. Sci. USA*, **99**, 16243–16248.
Mayer, B. J. (2001). *J. Cell Sci.* **114**, 1253–1263.
McRee, D. E. (1999). *J. Struct. Biol.* **125**, 156–165.
Moncalian, G., Cardenes, N., Deribe, Y. L., Spinola-Amilibia, M., Dikic, I. & Bravo, J. (2006). *J. Biol. Chem.* **281**, 38845–38853.
Musacchio, A., Noble, M., Pauptit, R., Wierenga, R. & Saraste, M. (1992). *Nature (London)*, **359**, 851–855.
Musacchio, A., Saraste, M. & Wilmanns, M. (1994). *Nature Struct. Biol.* **1**, 546–551.
Nishida, M., Nagata, K., Hachimori, Y., Horiuchi, M., Ogura, K., Mandiyan, V., Schlessinger, J. & Inagaki, F. (2001). *EMBO J.* **20**, 2995–3007.
Noble, M. E., Musacchio, A., Saraste, M., Courtneidge, S. A. & Wierenga, R. K. (1993). *EMBO J.* **12**, 2617–2624.
Otwinowski, Z. & Minor, W. (1997). *Methods Enzymol.* **276**, 307–326.
Pohl, E., Goranson-Siekierke, J., Choi, M. K., Roosild, T., Holmes, R. K. & Hol, W. G. J. (2001). *Acta Cryst.* D**57**, 619–627.
Qiu, X., Pohl, E., Holmes, R. K. & Hol, W. G. J. (1996). *Biochemistry*, **35**, 12292–12302.
Romir, J., Lilie, H., Egerer-Sieber, C., Bauer, F., Sticht, H. & Muller, Y. A. (2007). *J. Mol. Biol.* **365**, 1417–1428.
Safdar, A. & Rolston, K. V. (2007). *Clin. Infect. Dis.* **45**, 1602–1609.
Siderovski, D. P. & Willard, F. S. (2005). *Int. J. Biol. Sci.* **1**, 51–66.
Stols, L., Gu, M., Dieckman, L., Raffen, R., Collart, F. R. & Donnelly, M. I. (2001). *Protein Expr. Purif.* **25**, 8–15.
Terwilliger, T. C. & Berendzen, J. (1999). *Acta Cryst.* D**55**, 849–861.
Velayudhan, J., Hughes, N. J., McColm, A. A., Bagshaw, J., Clayton, C. L., Andrews, S. C. & Kelly, D. J. (2000). *Mol. Microbiol.* **37**, 274–286.
Whisstock, J. C. & Lesk, A. M. (1999). *Trends Biol. Sci.* **24**, 132–133.
Wylie, G. P., Rangachari, V., Bienkiewicz, E. A., Marin, V., Bhattacharya, N., Love, J. F., Murphy, J. R. & Logan, T. M. (2005). *Biochemistry*, **44**, 40–51.